Supporting Information for

Thermo- and Light-triggered Reversible Interconversion of Dysprosium-anthracene Complex and Their Responsive Optical, Magnetic and Dielectric properties

Xin-Da Huang, Ge-Hua Wen, Song-Song Bao, Jia-Ge Jia and Li-Min Zheng*

State Key Laboratory of Coordination Chemistry, School of Chemistry and Chemical Engineering, Collaborative Innovation Center of Advanced Microstructures, Nanjing University, Nanjing 210023, P. R. China.

E-mail: lmzheng@nju.edu.cn

Experimental section

General materials and measurements. The raw material 9-diethyl-phosphonomethylanthracene (depma) was synthesized according to the literature.[1] All other starting materials were of analytical grade obtained from commercial sources and used without any purification. PE 240C analyser were carried out to do the elemental analyses for C, H and N. The instrument to collect powder X-ray diffraction (PXRD) data was Bruker D8 advance diffractometer with Cu-Kα radiation in a range of 5-50°. The Fourier infrared spectra were attained from Bruker Tensor 27 spectrometer in 4000-600 cm^{-1} region by using ATR accessory. Thermogravimetric (TG) analyses were collected on a Mettler Toledo TGA/DSC 1 instrument in the range of 30-600 °C under a nitrogen flow (20 mL/min) at a heating rate of 5 °C min^{-1}. The determination of differential scanning calorimetry (DSC) was conducted on Mettler DSC823e instrument. The UV/Vis spectra were measured on a Perkin Elmer Lambda 950 UV/VIS/NIR spectrometer using powder samples.

X-ray Crystallography. Single crystals were used for data collections on a Bruker D8 Venture diffractometer using graphite-monochromated Mo-Kα radiation (λ = 0.71073 Å). The data were integrated using the Siemens SAINT program,[2] with the intensities corrected for Lorentz factor, polarization, air absorption, and absorption due to variation in the path length through the detector faceplate. Empirical absorption corrections were applied using the SADABS program.[3] The structures were solved by direct method and refined on F^2 by full-matrix least squares using SHELXTL.[4] All the non-hydrogen atoms were refined anisotropically. All hydrogen atoms were located in a difference map, added geometrically, and isotropically refined with a riding model. The residual electron densities were of no chemical significance. CCDC 2014614-2014615 contain the supplementary crystallographic data for this paper. These data can be obtained free of charge from the Cambridge Crystallographic Data Centre via www.ccdc.cam.ac.uk/data_request/cif.

Luminescent measurement. The steady photoluminescent spectra were attained at Bruker Spectrofluorimeter LS55. Time-resolved emission decays were carried out on Fluorolog-3 spectrofluorometer (Horiba Scientific). Nanosecond lifetime decays were conducted using a TCSPC MCA model equipped with a picosecond photodetector (<200 ps) (PPD850) and picosecond laser (duration is 180 ps, Deltadiode, 100 MHz laser). Microsecond lifetime decays were collected by a MCS mode on TCSPC HUB (DeltaHUB) with a LED source (SpectraLED) as a sample excitation source.

Magnetic measurement. The static and alternative current (ac) magnetic data were collected on ground polycrystalline samples using Quantum Design vibrating sample magnetometer (VSM). The hysteresis curves were recorded in each stable field. A drop of liquid Paraffin about 0.8 mg was added to avoid the movement and reorientation of samples during measurement.

The dc susceptibilities were corrected for diamagnetic contributions of both holder, paraffin and sample obtained from Pascal' s constants.[5]

Dielectric measurement. The 20 mg powder samples were pressed into pellets with diameter of 5 mm and thickness about 0.76 mm before deposited with silver conducting glue and then used for the dielectric measurements on the Broad Band Dielectric Spectrometer Concept80 in the temperature range of 193−323 K at frequency during 1.1-1328 kHz.

The synthesis method of $[Dy(SCN)_3(depma)_2(4\text{-}hpy)_2]$ (1). To a 5 mL methanol, $DyCl_3 \cdot 6H_2O$ (1 mmol) and KSCN (2 mmol) were added and stirred for 10 hour to precipitate the white powder of KCl prior to the filtration. Next, the methanol was distilled in vacuum so that the remainder was dissolved in 10 mL acetonitrile to obtain 0.1 mol/L solution of $Dy(SCN)_3$. Then, to a 1 mL 0.1 mol/L CH_3CN solution of $Dy(SCN)_3$, depma (0.2 mmol, 65.6 mg), 4-hpy (0.2 mmol, 19.5 mg) and another 2 mL CH_3CN were added and stirred for about 5 min. At last, with some yellow powder product filtered, the clear yellow solution was sealed and laid for two days to give block yellow crystals in yield of 50.4 mg (42.6%). The perfect crystals suitable for SC-XRD are obtained from the recrystallization from CH_3CN solution. Elemental anal. Calcd (%): C, 51.75; H, 4.42; N, 5.92. Found (%): C, 51.05; H, 4.77; N, 5.92. IR (cm^{-1}): 3233(w), 3119(vw), 3082(vw), 3051(w), 2980(w), 2942(vw), 2905(vw), 2862(vw), 2070(s), 1636(s), 1577(w), 1527(vs), 1445(vw), 1415(vw), 1389(m), 1343(vw), 1280(vw), 1259(vw), 1242(m), 1185(s), 1117(vw), 1098(vw), 1055(m), 1021(m), 998(w), 983 (w), 965 (vw), 928(vw), 894(vw), 861(w), 819(vw), 801(vw), 783(w), 732(m), 694(w), 603 (vw).

Table S1 Crystallographic data for compounds **1RT** and **1LT**.

	1RT	**1LT**
Empirical formula	$C_{51}H_{52}DyN_5O_8P_2S_3$	$C_{51}H_{52}DyN_5O_8P_2S_3$
Temperature (K)	300(2)	193(2)
Mw	1183.59	1183.59
Crystal system	Monoclinic	Triclinic
Space group	$P2_1/m$	$P\bar{1}$
a (Å)	10.081(4)	9.592(14)
b (Å)	24.946(8)	11.701(19)
c (Å)	11.246(4)	26.20(4)
α (°)	90	90.03(7)
β (°)	107.460(10)	91.86(4)
γ (°)	90	112.38(7)
V (Å^3)	2697.7(15)	2717(8)
Z	2	2
ρ_{calcd} (g cm^{-3})	1.457	1.447
F(000)	1202	1202
goodness-of-fit on F^2	1.048	1.087
R_1, wR_2 [$I > 2\sigma(I)$][a]	0.0456, 0.1111	0.1088, 0.2531
R_1, wR_2 (all data)[a]	0.0592, 0.1201	0.1557, 0.2777
CCDC number	2014614	2014615

[a] $R_1 = \Sigma||F_o| - |F_c||/\Sigma|F_o|$, $wR_2 = [\Sigma w(F_o^2 - F_c^2)^2/\Sigma w(F_o^2)^2]^{1/2}$

Table S2 Continuous Shape Measure (CShM) analyses of dysprosium geometries for **1RT** with highest occupancy and **1LT** using the SHAPE2.1 Software.

Geometry	**Symmetry**	**1RT**	**1LT**
Heptagon	D_{7h}	33.7(3)	34.837
Hexagonal pyramid	C_{6v}	24.5(4)	21.728
Pentagonal bipyramid	D_{5h}	0.96(4)	2.019
Capped octahedron	C_{3v}	5.5(7)	3.322
Capped trigonal prism	C_{2v}	4.2(6)	2.371
Johnson pentagonal bipyramid J13	D_{5h}	3.4(1)	4.565
Johnson elongated triangular pyramid J7	C_{3v}	21.6(2)	21.271

Table S3 Selected bond lengths (Å) and bond angles (°) for **1RT** at 300 K and **1LT** at 193 K.

1RT		**1LT**	
Dy1-O1A	2.312(4)	Dy1-O1	2.356(11)
Dy1-O1	2.312(4)	Dy1-O4	2.347(12)
Dy1-O4/O4'	2.246(12)/2.188(15)	Dy1-O7	2.258(13)
Dy1-O5/O5A	2.207(6)	Dy1-O8	2.251(12)
Dy1-N1	2.433(5)	Dy1-N1	2.473(17)
Dy1-N1A	2.433(5)	Dy1-N2	2.450(14)
Dy1-N3	2.401(7)	Dy1-N3	2.489(14)
O1-Dy1-O1A	141.24(17)	O1-Dy1-O4	137.3(4)
O1A-Dy1-O4/O4'	85.35(16)/81.88(17)	O1-Dy1-O7	81.9(4)
O1A-Dy1-O5/O5A	97.2(5)/95.3(5)	O1-Dy1-O8	94.6(4)
O1A-Dy1-N1	73.09(17)	O1-Dy1-N1	76.0(5)
O1A-Dy1-N1A	144.10(16)	O1-Dy1-N2	148.4(4)
O1A-Dy1-N2	72.91(11)	O1-Dy1-N3	73.7(4)
O1-Dy1-O4/O4'	85.35(16)/81.88(17)	O4-Dy1-O7	79.8(4)
O1-Dy1-O5/O5A	95.3(5)/97.2(5)	O4-Dy1-O8	106.1(5)
O1-Dy1-N1	144.10(16)	O4-Dy1-N1	139.4(5)
O1-Dy1-N1A	73.09(17)	O4-Dy1-N2	72.4(4)
O1-Dy1-N2	72.91(11)	O4-Dy1-N3	73.5(5)
O4/O4'-Dy1-O5/O5A	174.9(3)/173.9(4)	O7-Dy1-O8	173.8(4)
O4/O4'-Dy1-N1	88.8(3)/97.8(3)	O7-Dy1-N1	85.0(5)
O4/O4'-Dy1-N1A	88.8(3)/97.8(3)	O7-Dy1-N2	97.0(4)
O4/O4'-Dy1-N2	103.5(4)/92.5(4)	O7-Dy1-N3	103.3(5)
O5/O5A-Dy1-N1	87.6(3)/86.5(3)	O8-Dy1-N1	89.2(5)
O5/O5A-Dy1-N1A	86.5(3)/87.6(3)	O8-Dy1-N2	83.2(5)
O5/O5A-Dy1-N2	81.5(3)/81.5(3)	O8-Dy1-N3	80.5(5)
N1-Dy1-N1A	71.7(2)	N1-Dy1-N2	72.4(5)
N1-Dy1-N2	142.57(13)	N1-Dy1-N3	147.0(5)
N1A -Dy1-N2	142.57(13)	N2-Dy1-N3	136.1(5)

Symmetry code: A = x, 1/2-y, z

Table S4 The parameters of intermolecular hydrogen bonds for **1RT** and **1LT**.

Phase	D-H···A	$d_{H\cdots A}$ (Å)	$d_{D\cdots A}$ (Å)	$Angle_{D\text{-}H\cdots A}$ (º)
1RT	N3-H3N···N1/N1A	2.70	3.46	148
	N4-H4N···S1	2.82	3.45	132
	N3'-H3N'···S2	2.03	2.63	126
1LT	C39-H39···C49	2.88	3.55	129
	N4-H4N···S3	2.49	3.26	148
	N5-H5N···S3	2.82	3.42	128
	C48-H48···S3	2.82	3.45	125

Table S5 The transient luminescent lifetime (τ) at room temperature for compounds **1RT**, **1LT** and **1UV** excited at 375 nm for short nanosecond lifetime and 370 nm for long microsecond lifetime. To obtain the lifetime, their decay profiles are fitted reasonably to a single or double exponential function using the software DAS6 attached to FluoroLog-UltraFast (HORIBA Instrument Inc, Edison).

Compound	λ_{em} / nm	τ_1 / ns	τ_2 / ns	$\tau_{average}$ / ns	χ^2
1RT	535	37.3			1.10
1LT	530	44.7			1.07
1UV	424	0.62 (38.68%)	2.67 (61.32%)	1.17	1.05
	446	0.70 (38.17%)	3.01 (61.83%)	1.34	1.18
	485	21.2 µs			0.99
	535	2.96 (9.29%)	36.5 (90.71%)	17.8	1.18
	575	20.7 µs			1.10

Table S6 The fit parameters obtained from analyses of the ac susceptibilities of **1** under zero bias dc field.

T / K	χ_T / cm^3 mol^{-1}	χ_S / cm^3 mol^{-1}	ln(τ / s)	α	$R^2 \times 10^{-4}$
2.0	7.60	0.36	-4.28	0.31	5.67
3.0	4.89	0.26	-4.52	0.30	5.53
4.0	3.59	0.22	-4.72	0.29	5.60
5.0	2.83	0.20	-4.92	0.26	6.06
6.0	2.33	0.19	-5.17	0.22	6.12
7.0	1.96	0.19	-5.54	0.17	4.92
8.0	1.70	0.17	-5.99	0.13	2.67
9.0	1.50	0.16	-6.55	0.10	1.33
9.5	1.42	0.15	-6.88	0.09	0.91
10.0	1.34	0.15	-7.25	0.09	0.71
10.5	1.28	0.15	-7.66	0.08	0.49
11.0	1.22	0.15	-8.10	0.08	0.27
11.5	1.16	0.14	-8.59	0.09	0.43
12.0	1.11	0.10	-9.12	0.09	0.33

Table S7 The fit parameters obtained from analyses of the ac susceptibilities of **1** under different dc field at 6 K.

Field / kOe	χ_T / cm^3 mol^{-1}	χ_S / cm^3 mol^{-1}	ln(τ / s)	α	$R^2 \times 10^{-3}$
0	2.11	0.18	-5.17	0.22	0.62
0.25	2.50	0.17	-4.29	0.37	1.27
0.50	2.45	0.22	-3.39	0.27	2.78
0.75	2.37	0.17	-3.18	0.19	1.18
1.00	2.29	0.14	-3.12	0.16	1.47
1.50	2.25	0.12	-3.20	0.16	1.72
2.00	2.19	0.12	-3.26	0.17	2.93

Table S8 The fit parameters obtained from analyses of the ac susceptibilities of **1** under 1 kOe bias dc field.

T / K	χ_T / cm^3 mol^{-1}	χ_S / cm^3 mol^{-1}	ln(τ / s)	α	$R^2 \times 10^{-4}$
5.0	2.47	0.12	-2.04	0.22	26.9
6.0	2.20	0.11	-3.05	0.19	8.89
7.0	1.81	0.10	-4.12	0.12	15.7
8.0	1.53	0.10	-5.03	0.10	6.82
9.0	1.38	0.10	-5.88	0.10	3.05
9.5	1.30	0.11	-6.35	0.09	7.77
10.0	1.24	0.11	-6.84	0.10	9.08
10.5	1.17	0.12	-7.36	0.09	3.49
11.0	1.14	0.07	-7.94	0.14	10.0
11.5	1.08	0.09	-8.47	0.12	5.09
12.0	1.03	0.05	-9.10	0.12	6.19

Table S9 The fit parameters obtained from analyses of the ac susceptibilities of **1UV** under zero bias dc field.

T / K	χ_T / cm^3 mol^{-1}	χ_S / cm^3 mol^{-1}	ln(τ / s)	α	$R^2 \times 10^{-5}$
2.0	6.29	0.89	-6.58	0.27	10.6
2.5	4.97	0.74	-6.65	0.27	11.2
3.0	4.12	0.63	-6.72	0.26	10.3
3.5	3.51	0.56	-6.79	0.26	11.4
4.0	3.06	0.50	-6.89	0.25	9.44
4.5	2.70	0.47	-7.02	0.24	9.75
5.0	2.43	0.43	-7.19	0.24	8.91
5.5	2.20	0.40	-7.38	0.23	6.02
6.0	2.01	0.37	-7.62	0.23	4.85
6.5	1.85	0.34	-7.87	0.23	4.72
7.0	1.72	0.31	-8.16	0.24	4.43
7.5	1.60	0.29	-8.47	0.25	4.24
8.0	1.50	0.20	-8.91	0.26	3.97

Table S10 The fit parameters obtained from analyses of the ac susceptibilities of **1UV** under different dc field at 5 K.

Field / kOe	χ_T / cm^3 mol^{-1}	χ_S / cm^3 mol^{-1}	ln(τ / s)	α	$R^2 \times 10^{-3}$
0	2.91	0.45	-7.12	0.24	0.22
0.25	3.01	0.44	-5.96	0.40	0.70
0.50	3.00	0.38	-4.54	0.35	0.58
0.75	2.95	0.24	-4.04	0.37	0.36
1.00	2.95	0.19	-3.90	0.37	2.09
1.50	2.67	0.18	-4.14	0.33	1.30
2.00	2.61	0.18	-4.12	0.31	6.78

Table S11 The fit parameters obtained from analyses of the ac susceptibilities of **1UV** under 1 kOe dc field.

T / K	χ_T / cm^3 mol^{-1}	χ_S / cm^3 mol^{-1}	ln(τ / s)	α	$R^2 \times 10^{-4}$
4.0	3.64	0.25	-2.34	0.38	11.5
4.5	3.23	0.22	-3.18	0.36	6.01
5.0	2.84	0.21	-4.04	0.34	8.98
5.5	2.67	0.20	-4.64	0.34	6.33
6.0	2.41	0.19	-5.25	0.34	3.52
6.5	2.21	0.19	-5.87	0.33	3.83
7.0	2.03	0.21	-6.47	0.30	4.77
7.5	1.89	0.21	-7.01	0.29	3.65
8.0	1.76	0.24	-7.52	0.26	4.28
8.5	1.66	0.20	-8.09	0.29	3.46
9.0	1.57	0.20	-8.60	0.28	1.99

Table S12 The fit parameters obtained from analyses of the ac susceptibilities of **1R** under zero bias dc field.

T / K	χ_T / cm^3 mol^{-1}	χ_S / cm^3 mol^{-1}	ln(τ / s)	α	$R^2 \times 10^{-4}$
2.0	7.09	0.31	-4.25	0.32	5.00
3.0	4.57	0.22	-4.50	0.30	4.67
4.0	3.37	0.19	-4.69	0.29	4.76
5.0	2.66	0.18	-4.88	0.26	5.70
6.0	2.18	0.17	-5.14	0.22	6.34
7.0	1.84	0.17	-5.50	0.17	5.53
8.0	1.59	0.16	-5.95	0.13	3.06
9.0	1.41	0.14	-6.49	0.10	1.49
9.5	1.33	0.14	-6.81	0.09	0.99
10.0	1.26	0.14	-7.18	0.09	2.30
10.5	1.20	0.14	-7.57	0.08	0.55
11.0	1.14	0.15	-7.99	0.07	0.46
11.5	1.09	0.12	-8.50	0.09	0.51
12.0	1.04	0.05	-9.11	0.10	0.61

Table S13 All light-responsive Ln-SMMs through photochemical reactions.

Compounds	Hysteresis	reversibility	Field / KOe	U_{eff} / K	τ_0 / s	Ref.
$[Cu^{II}_2Tb^{III}_2(L^1)_2(NO_3)_2(dae\text{-}o)_2]\cdot 2(n\text{-}BuOH)$	no	no	0	14.91	2.39×10^{-7}	6
			1.0	23.76	7.00×10^{-8}	
$[Cu^{II}_2Tb^{III}_2(L^1)_2(NO_3)_2(dae\text{-}c)_2]\cdot 2(n\text{-}BuOH)$			0	8.44	9.30×10^{-6}	
			1.0	22.59	9.07×10^{-8}	
$\{[Cu^{II}Tb^{III}(L^1)(n\text{-}BuOH)_{0.5}]_2(dae\text{-}c)_3\}\cdot 5(DMF)\cdot 4(n\text{-}BuOH)\cdot 2(H_2O)$	no	no	0	12.13	3.03×10^{-6}	
			1.0	22.04	2.11×10^{-7}	
$\{[Cu^{II}Tb^{III}(L^1)(n\text{-}BuOH)_{0.5}]_2(dae\text{-}o)_3\}\cdot 5(DMF)\cdot 4(n\text{-}BuOH)\cdot 2(H_2O)$			0	13.46	5.27×10^{-7}	
			1.0	23.94	1.33×10^{-8}	
$\{Dy_2(dae\text{-}o)_3(bpy)_2(H_2O)_2\}_n$	no	no	0	14.5	5.33×10^{-6}	7
			1	21.7	8.1×10^{-7}	
$\{Dy_2(dae\text{-}c)_3(bpy)_2(H_2O)_2\}_n$			1.0	17.1	1.9×10^{-6}	
$[\{Dy_2(dae\text{-}o)_3(DMSO)_3(MeOH)\}\cdot 10MeOH]_n$	no	no	1.0	14.2	1.9×10^{-8}	8
$[\{Dy_2(dae\text{-}c)_3(DMSO)_3(MeOH)\}\cdot 10MeOH]_n$			1.0	14.7	7.25×10^{-9}	
$[Dy(Tp^{py})F(L^2{}_c)]PF_6$	yes	yes	0	225.9	7.7×10^{-7}	9
$[Dy(Tp^{py})F(L^2{}_o)]PF_6$			0	225.9	7.7×10^{-7}	
$[Dy(trans\text{-}L^3{}_{MC})(OTf)_2(H_2O)_2]OTf$	no	no	1.2	32.9	1.24×10^{-5}	10
$[Dy(cis\text{-}L^3{}_{MC})(OTf)_2(H_2O)_2]OTf$			1.2	32.9	5.76×10^{-5}	
$[Dy(bpe)(H_2O)_4(NO_3)_2](NO_3)\cdot 2bpe$	no	no	0	55.1	9.81×10^{-9}	11
			0.3	56.7	9.81×10^{-9}	
$[Dy_2(tpcb)(H_2O)_8(NO_3)_4](NO_3)_2\cdot 2bpe\cdot tpcb$			0.4	47.9	1.22 × 10-9	
$(Hbpe)_2[Dy(bpe)(H_2O)(4\text{-}pyO)(NO_3)(SCN)_3]SCN$	yes	no	0	153.8	5.54 ×	12
			1.5	201.9	1.18 ×	
$(Hbpe)_2[Dy(bpe)(H_2O)(4\text{-}pyO)(NO_3)(SCN)_3]SCN$			0	205.5	2.08 ×	
			1.5	234.5	1.91 ×	
$[Er(nat)_3\cdot MeOH\cdot bpe]$	no	no	0.8	30.7	3.8×10^{-10}	13
$[\{Er(nat)_3\ MeOH\}_2(tpcb)]$			0.8	21.6	2.1×10^{-9}	
$DySc_2N@C_{80}@[Zr_6O_4(OH)_4L^4{}_6]_n$	yes	no	unknown			14
$[Dy_3(HHEDP)_3(H_2HEDP)_3]\cdot 2H_3TPT\cdot H_4HEDP\cdot 10H_2O$	no	yes	no			15
$[Dy_3(HHEDP)_3(H_2HEDP)_3]\cdot 2H_3TPT\cdot H_4HEDP\cdot 10H_2O$			0	108.1	1.5×10^{-9}	
$[Dy(depma)(hmpa)_2(NO_3)_3]$	no	yes	0.5	20.4	1.58×10^{-8}	16
$[Dy_2(depma_2)(hmpa)_4(NO_3)_6]$			0.5	43.2	5.12×10^{-9}	
$[Dy(depma)(temdp)(NO_3)_3]$	no	no	0.75	17.4	4.2×10^{-8}	17
$[Dy_2(depma_2)(temdp)_2(NO_3)_6]$			0.75	5.5	3.6×10^{-5}	
$[Dy(dmpma)(temdp)(NO_3)_3]$	no	no	1.0	24.1	5.2×10^{-10}	
$[Dy_2(dmpma_2)(temdp)_2(NO_3)_6]$			1.0	55.0	4.3×10^{-9}	

$[Dy^{III}(SCN)_3(depma)_2(4\text{-}hpy)_2]$	yes	yes	0	141	1.1×10^{-9}	This work
			1	181	4×10^{-11}	
$\{Dy^{III}(SCN)_3(depma_2)(4\text{-}hpy)_2\}$			0	101	1.0×10^{-9}	
			1	123	1.0×10^{-9}	

H_2L^1 = 1,3-bis((3-methoxysalicylidene)amino)propane, H_2dae = 1,2-bis(5-caxboxyl-2-methyl-3-thienyl)perfluorocyclopentene with open and closed isomer, bpy = 2, 2' – bipyridine, Tp^{py} = tris(3-(2-pyridyl)pyrazolyl)hydroborate, L^2 = bispyridyl dithienylethene with open and closed form, L^3_{MC} = merocyanine-based ligand with trans- and cis-isomer, bpe = 1,2-bis(4-pyridyl)ethane, tpcb = tetrakis(4-pyridyl)cyclobutane, nat = 4,4,4-trifluoro-1-(2-naphthyl)-1,3-butanedione, H_2L^4 = 2'-phenyldiazenyl-1,1':4',1''-terphenyl-4,4''-dicarboxylate, H_4HEDP = hydroxyethylidene diphosphonate; TPT = 2,4,6-tri(4-pyridyl)-1,3,5-triazine, hmpa = Hexamethylphosphoramide, depma = 9-diethylphosphonomethylanthracene, $depma_2$ = the [4+4] photodimer of ligand depma, temdp = tetraethyl methylenediphosphonate, dmpma = 9-dimethylphosphonomethylanthracene, $dmpma_2$ = the [4+4] photodimer of ligand dmpma.

References:

1 D. K. Cao, Y. W. Gu; J. Q. Feng, Z. S. Cai and M. D. Ward, *Dalton Trans*., 2013, **42**, 11436.

2 SAINT, Program for Data Extraction and Reduction, Siemens Analytical X-ray Instruments, Madison, WI, 1994–1996.

3 L. Krause, R. Herbst-Irmer, G.M. Sheldrick, D. Stalke, *J. Appl. Cryst*., 2015, **48**, 3-10.

4 a) SHELXTL (version 5.0), Reference Manual, Siemens Industrial Automation, Analytical Instruments, Madison, WI, 1995; b) Sheldrick, G. M. SHELXTL 5.10 for Windows NT: Structure Determination Software Programs, Bruker Analytical X-ray Systems, Inc., Madison, WI, 1997; c) G. M. Sheldrick, SHELXS-97 and SHELXL-97, Program for Crystal Structure Solution and Refinement; University of Göttingen: Göttingen, Germany,1997; d) G. M. Sheldrick, *Acta Crystallogr. Sect*. C, 2015, **71**, 3–8; e) G. M. Sheldrick, *Acta Crystallogr., Sect. A*: *Found. Crystallogr*., 2008, **64**, 112−122; f) Sheldrick, G. M. *Acta Crystallogr., Sect. A: Found*. *Adv*., 2015, **71**, 3−8.

5 O. Kahn, Molecular Magnetism, Wiley-VCH: New York., 1993.

6 T. Shiga, H. Miyasaka, M. Yamashita, M. Morimotob and M. Irie, *Dalton Trans.,* 2011, **40**, 2275–2282.

7 G. Cosquer, M. Morimoto, M. Irie, A. Fetoh, B. K. Breedlovea and M. Yamashita, *Dalton Trans.,* 2015, **44**, 5996–6002

8 D. Pinkowicz, M. Ren, L.-M. Zheng, S. Sato, M. Hasegawa, M. Morimoto, M. Irie, B. K. Breedlove, G. Cosquer, K. Katoh, and M. Yamashita, *Chem. Eur. J*., 2014, **20**, 12502 – 12513.

9 M. Hojorat, H. A. Sabea, L. Norel, K. Bernot, T. Roisnel, F. Gendron, B. L. Guennic, E. Trzop, E. Collet, J. R. Long, and S. Rigaut, *J. Am. Chem. Soc*., 2020, **142**, 931−936.

10 a) P. Selvanathan, G. Huang, T. Guizouarn, T. Roisnel, G. Fernandez-Garcia, F. Totti, B. L. Guennic, G. Calvez, K. Bernot L. Norel, and S. Rigaut, *Chem. Eur. J*., 2016, **22**, 15222-15226. b) P. Selvanathan, V. Dorcet, T. Roisnel, K. Bernot, G. Huang, B. L. Guennic, L. Norel and S. Rigaut, *Dalton Trans*., 2018, **47**, 4139–4148.

11 L.-F. Wang, J.-Z. Qiu, J.-L. Liu, Y.-C. Chen, J.-H. Jia, J. Jover, E. Ruiz and M.-L. Tong, *Chem. Commun*., 2015, **51**, 15358–15361.
12 L.-F. Wang, J.-Z. Qiu, Y.-C. Chen, J.-L. Liu, Q.-W. Li, J.-H. Jia and M.-L. Tong, *Inorg. Chem. Front*., 2017, **4**, 1311–1318.
13 J. Li, M. Kong, L. Yin, J. Zhang, F. Yu, Z.-W. Ouyang, Z. Wang, Y.-Q. Zhang and Y. Song, *Inorg. Chem*., 2019, **58**, 14440–14448.
14 H. Meng, C. Zhao, M. Nie, C. Wang and T. Wang, *ACS Appl. Mater. Interfaces,* 2018, **10**, 32607–32612.
15 Y.-J. Ma, J.-X. Hu, S.-D. Han, J. Pan, J.-H. Li, and G.-M. Wang, *J. Am. Chem. Soc*., 2020, **142**, 2682−2689.
16 X.-D. Huang, Y. Xu, K. Fan, S.-S. Bao, M. Kurmoo and L.-M. Zheng, *Angew. Chem. Int. Ed*., 2018, **57**, 8577–8581.
17 X.-D. Huang, J.-G. Jia, M. Kurmoo, S.-S. Bao and L.-M. Zheng, *Dalton Trans*., 2019, **48**, 13769–13779.

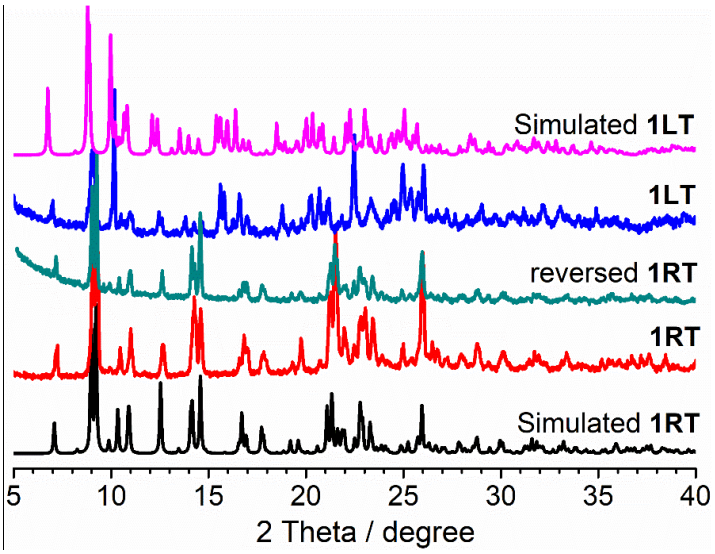

Fig. S1 The PXRD patterns collected at 20°C for powder samples of **1RT**, **1LT** and the reversed **1RT** after the thermal annealing of **1LT** at 40°C compared with their simulated patterns from corresponding crystal structures.

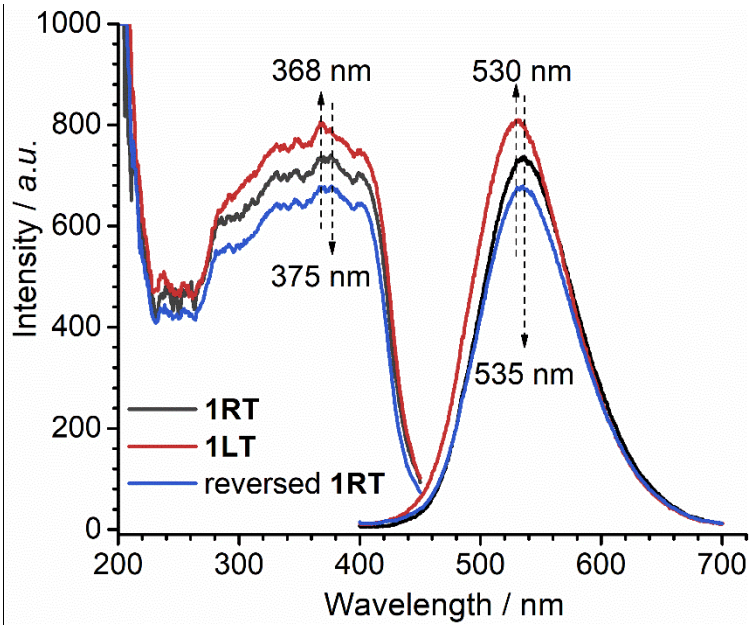

Fig. S2 The excitation and emission spectra for the thermal switching between **1RT** and **1LT** collected at 22°C.

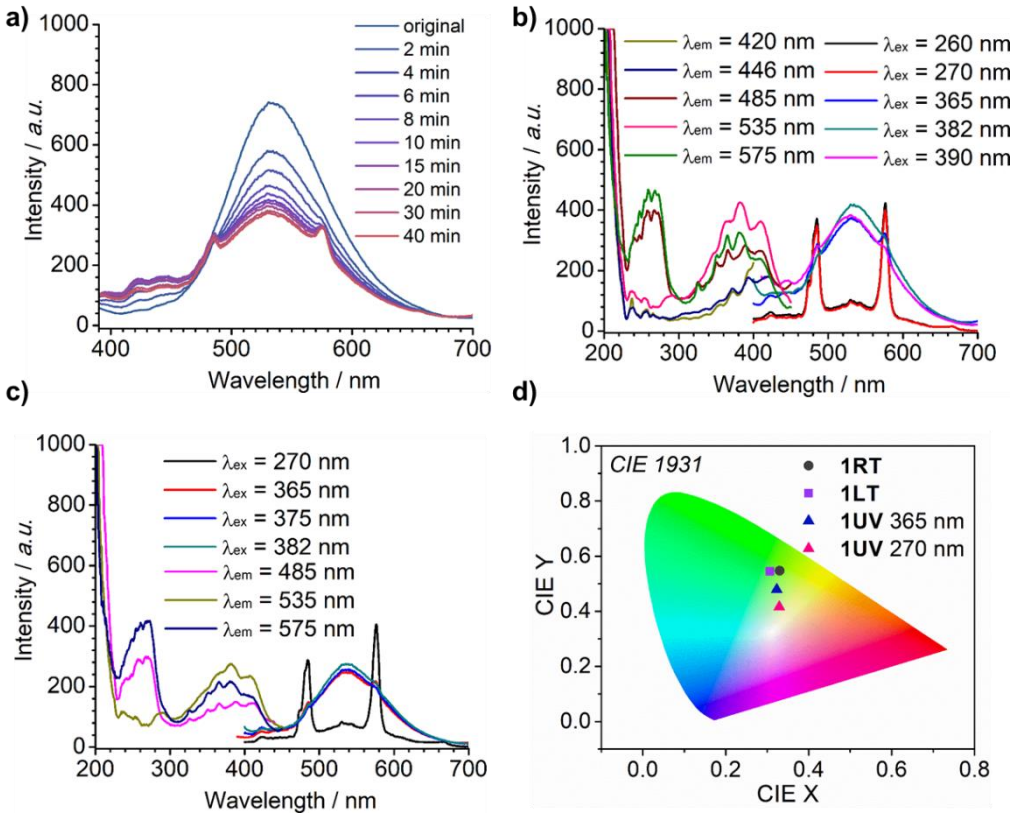

Fig. S3 a) The in-situ photoluminescence spectra excited at 365 nm as a function of irradiation time under 365 nm LED light in power of 185 mW/cm^2 during the transformation of 2 mg sample from **1RT** to **1UV**. b) The excitation and emission spectra for 2 mg sample of **1RT** after the exposure to 365 nm LED light for 40 min. c) The excitation and emission spectra of **1UV**. d) The 1931 CIE graphs of **1RT**, **1LT** and **1UV**.

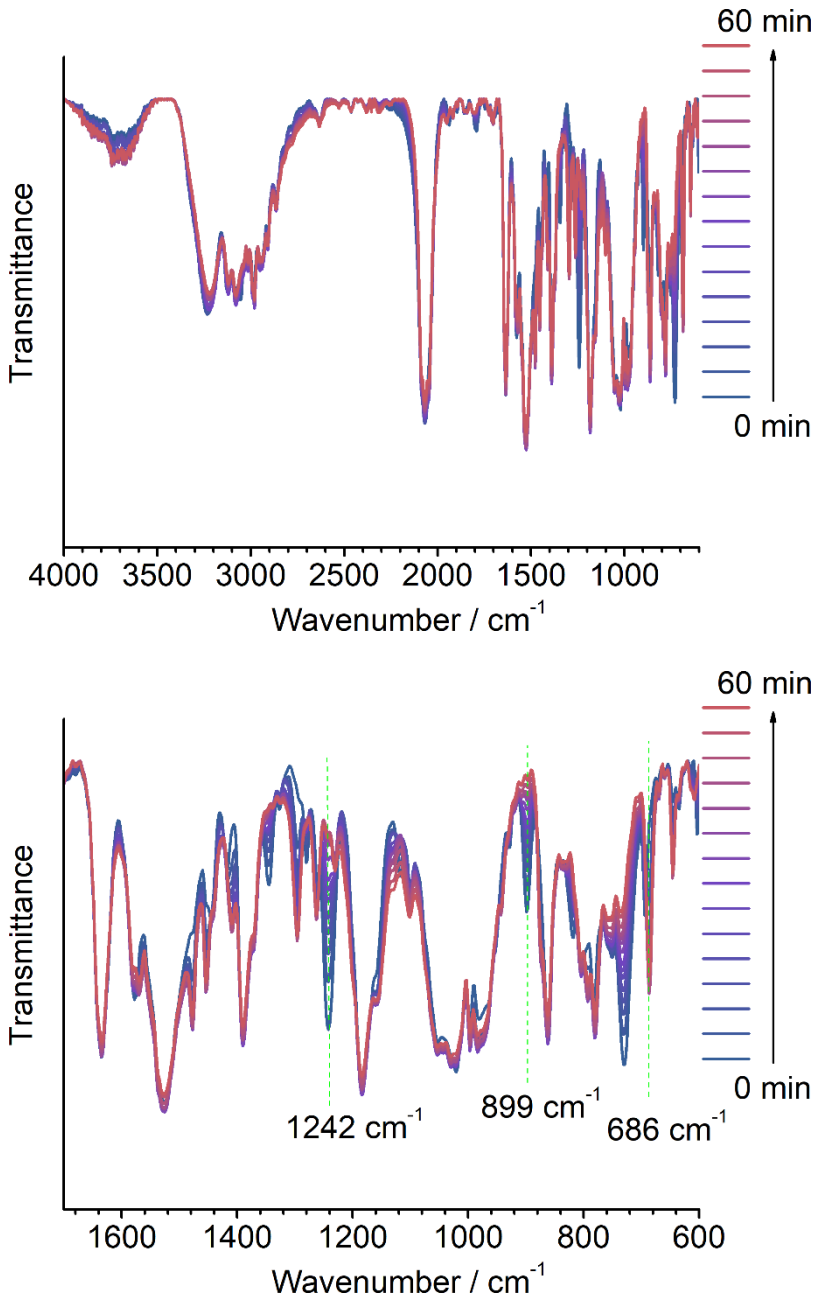

Fig. S4 Time-dependent in-situ IR spectra for **1RT** exposed to 365 nm UV light up to 1 hour shown in wavenumber range of 4000-600 cm^{-1} (up) and 1700-600 cm^{-1} (bottom).

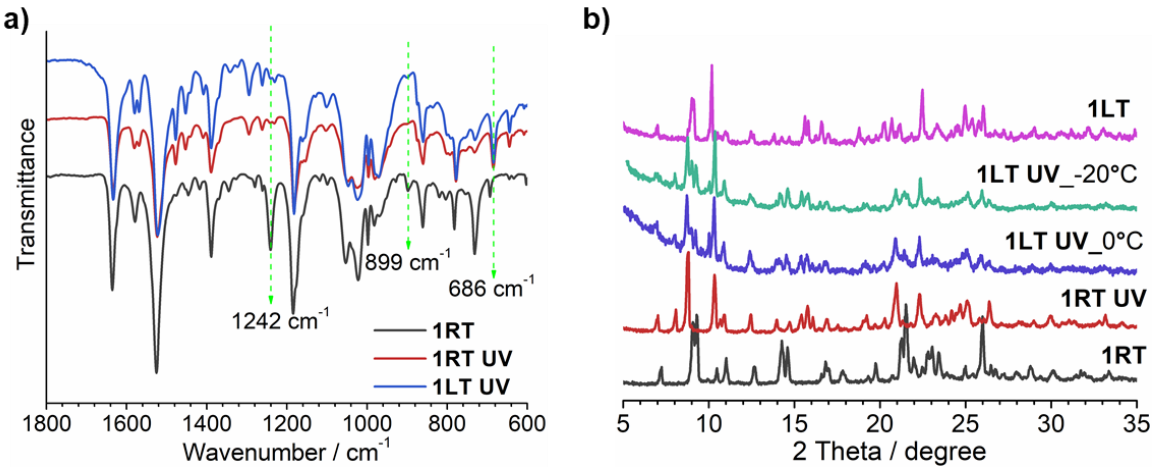

Fig. S5 The IR spectra and powder XRD patterns for **1RT**, **1LT** and their photodimerized products.

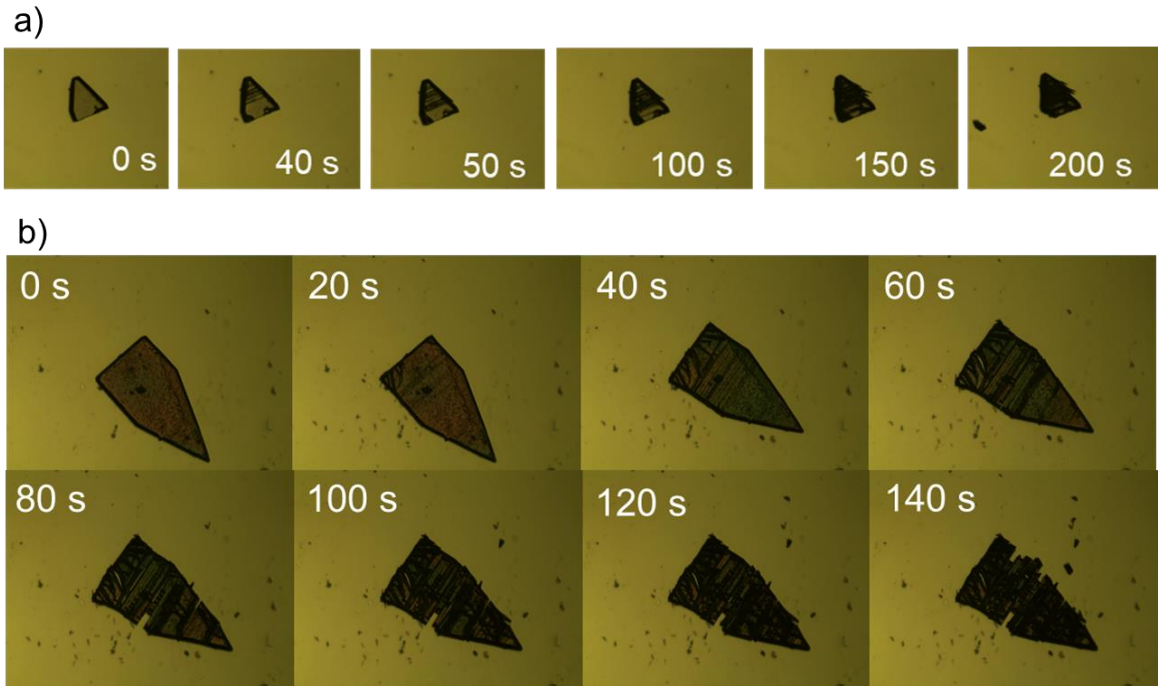

Fig. S6 The photographs showing the fragment of two plate crystals of **1RT** (a, b) exposed to LED UV light for different time.

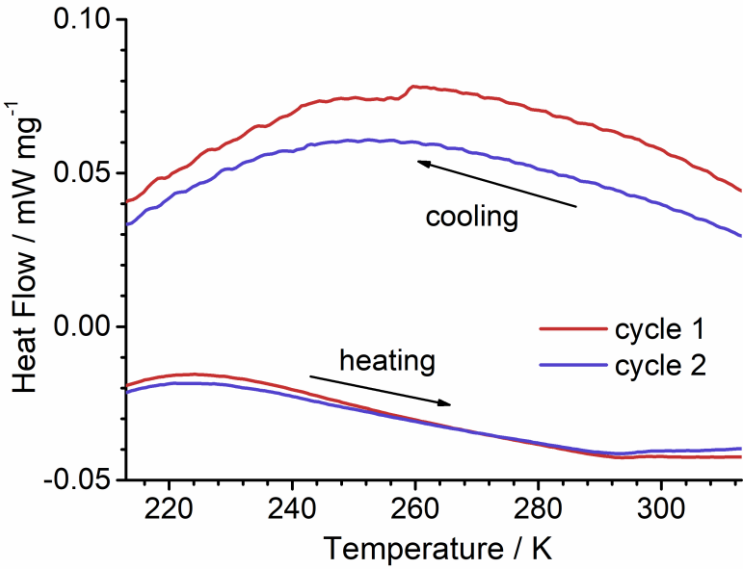

Fig. S7 The DSC curves of **1UV** collected between 193-323 K for two cooling-heating cycles at sweeping rate of 5 K/min under 150 mL/min N_2 atmosphere.

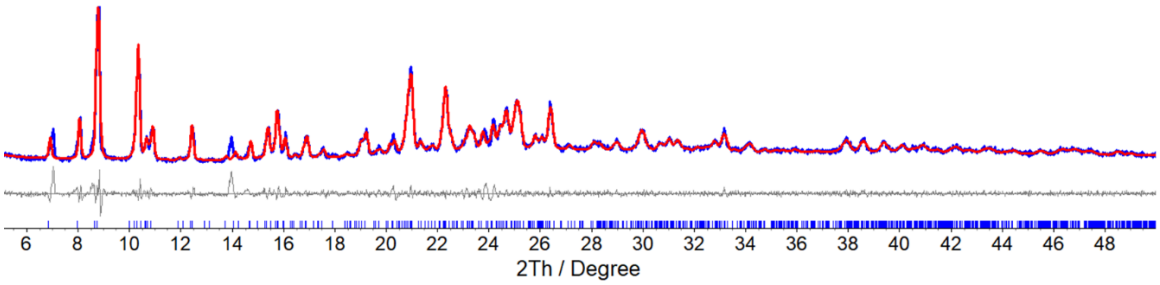

Fig. S8 The PXRD pattern of **1UV** (Rwp = 5.0%) refined by TOPAS software to determine the unit cell.

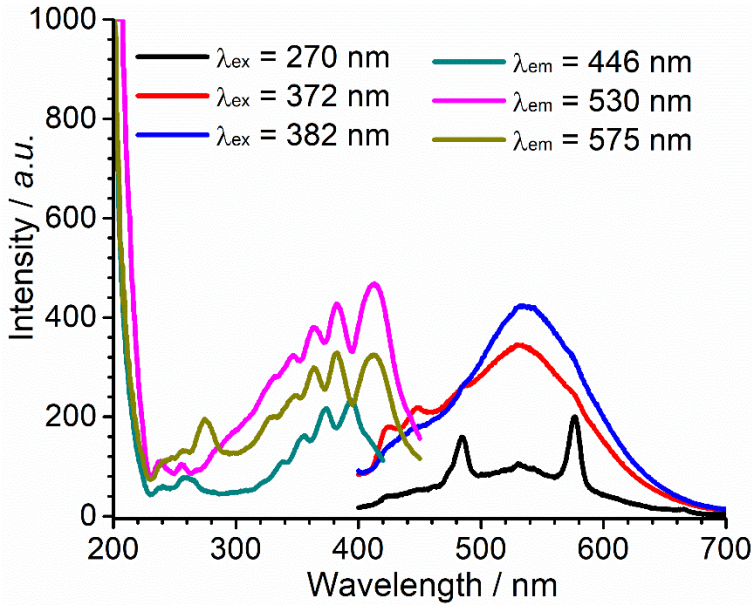

Fig. S9 Excitation and emission spectra of irradiation product of **1LT** at 273 K.

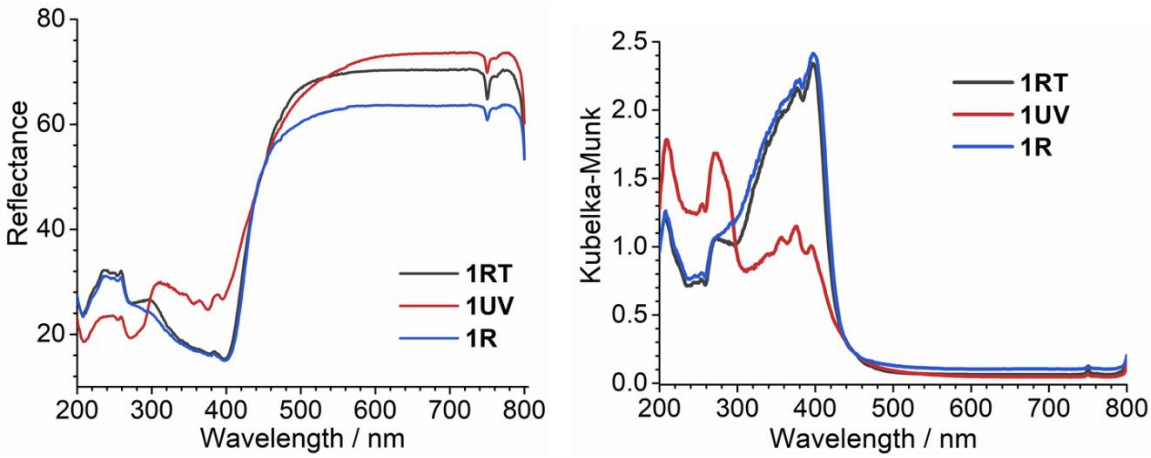

Fig. S10 The UV-vis diffused reflectance spectra (left) and corresponding Kubelka-Munk functions: $F(R)= (1-R)^2/2R$ (right) for **1RT**, **1UV** and **1R**.

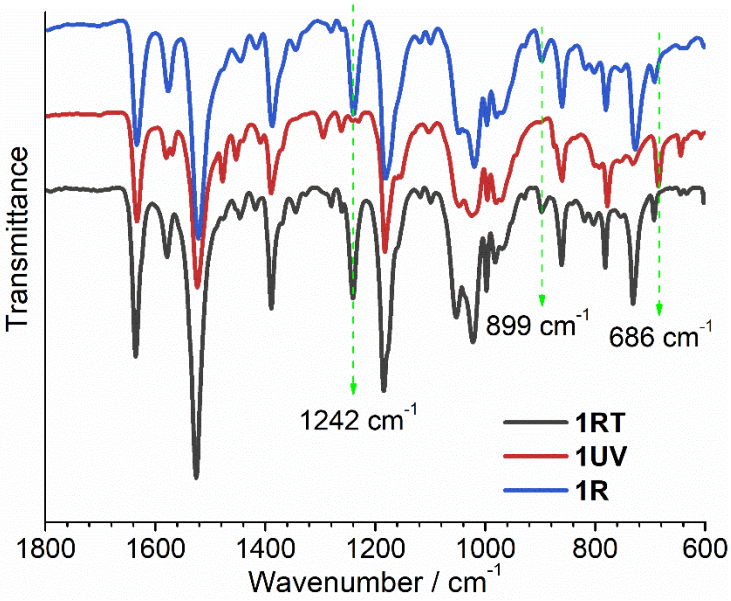

Fig. S11 The IR spectra of **1RT**, **1UV** and **1R**.

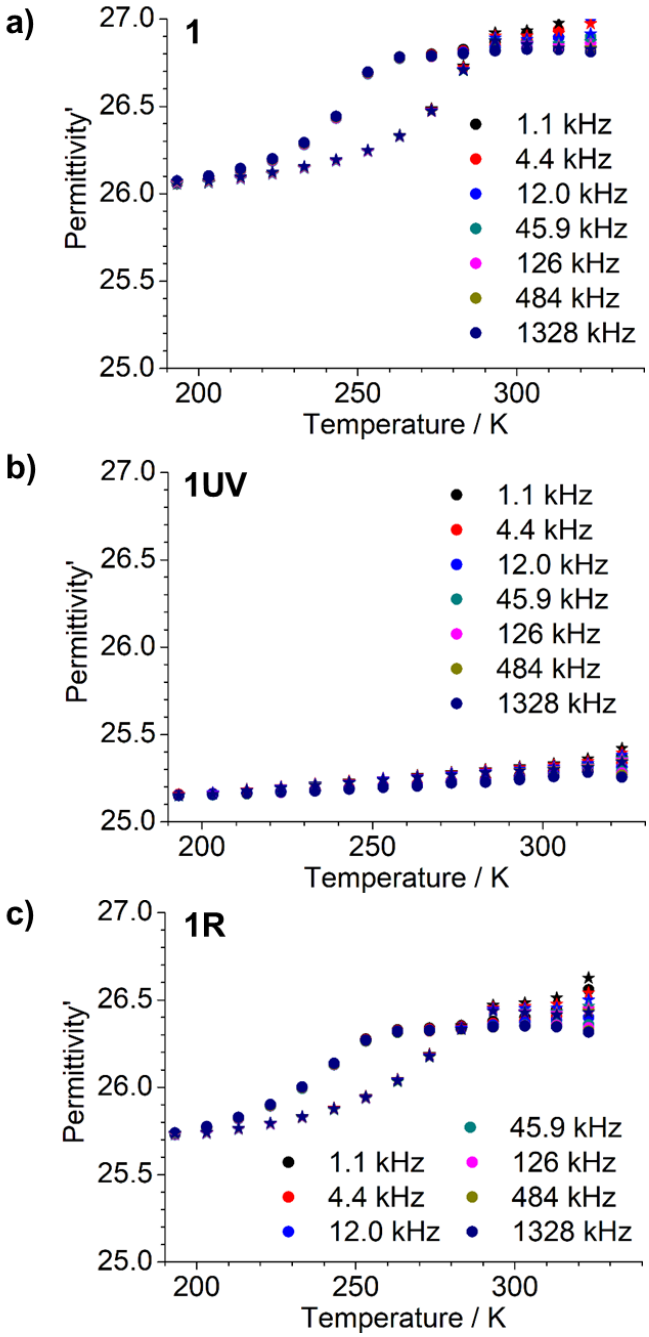

Fig. S12 The dielectric constants of **1** (a), **1UV** (b) and **1R** (c) between 193-323 K for one cooling (dot curve) and heating (star curves) cycle.

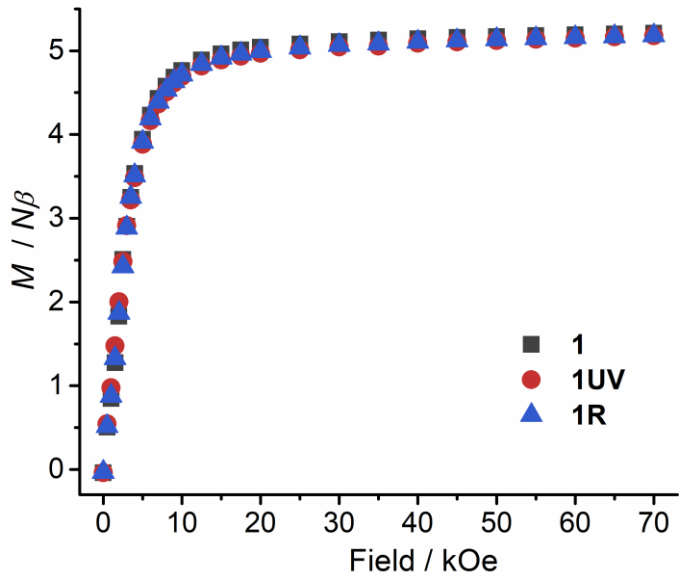

Fig. S13 The isothermal magnetization (*M*) for **1**, **1UV** and **1R** below 70 kOe dc field at 2 K.

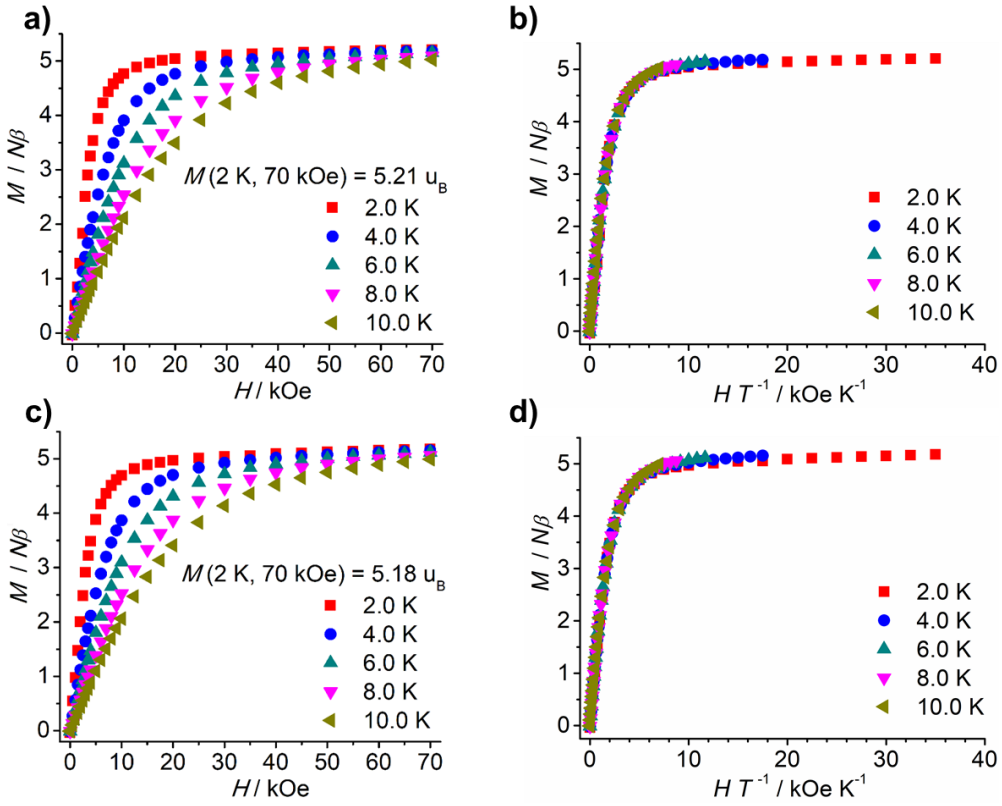

Fig. S14 The isothermal magnetization for **1LT** (a, b) and **1UV** (c, d) as a function of *H* and HT^{-1} at depicted temperatures.

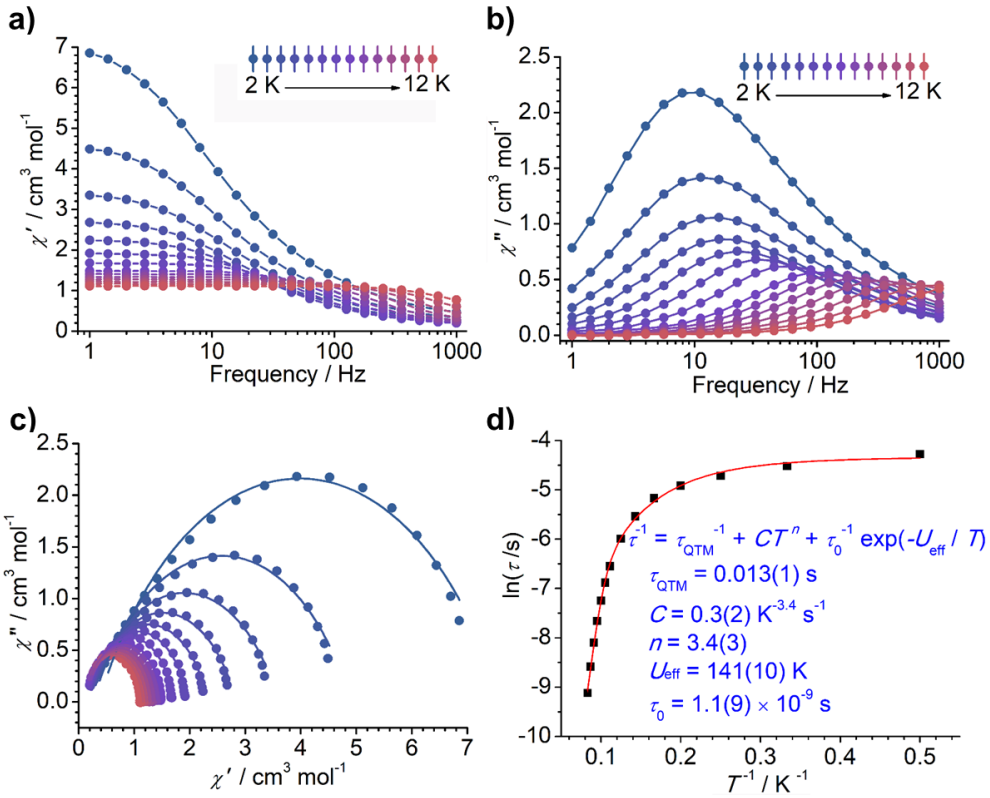

Fig. S15 The in-phase (a) and out-of-phase (b) ac susceptibilities, corresponding Cole-Cole plots (c) and relaxation time (d) of **1LT** under zero dc field below 12 K.

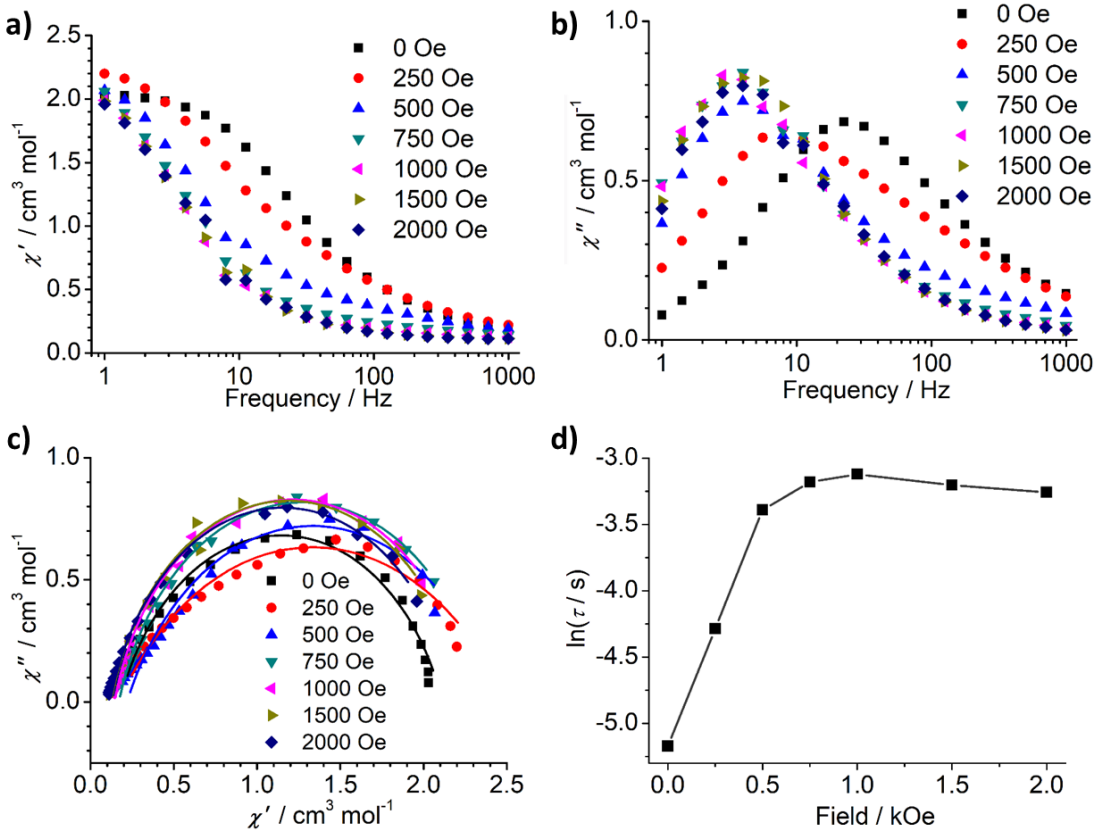

Fig.S16 The in-phase (a) and out-of-phase (b) ac susceptibilities, corresponding Cole-Cole plots (c) and relaxation time (d) of **1LT** at 6 K under different dc field.

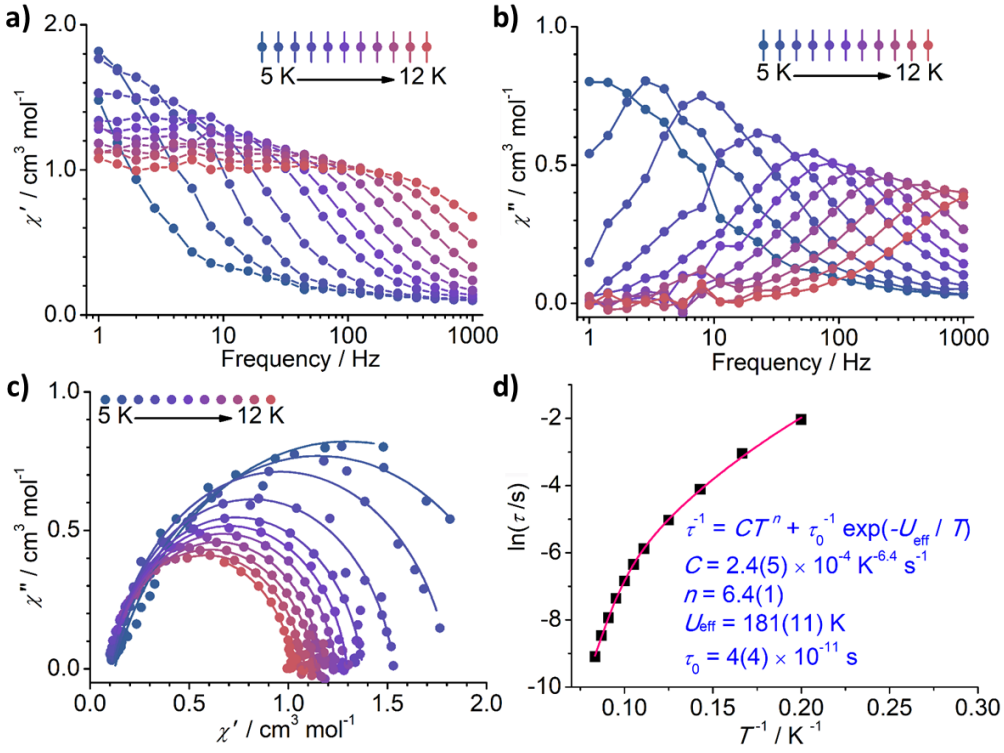

Fig. S17 The in-phase (a) and out-of-phase (b) ac susceptibilities, corresponding Cole-Cole plots (c) and relaxation time (d) of **1LT** under 1 kOe dc field between 5 and 12 K.

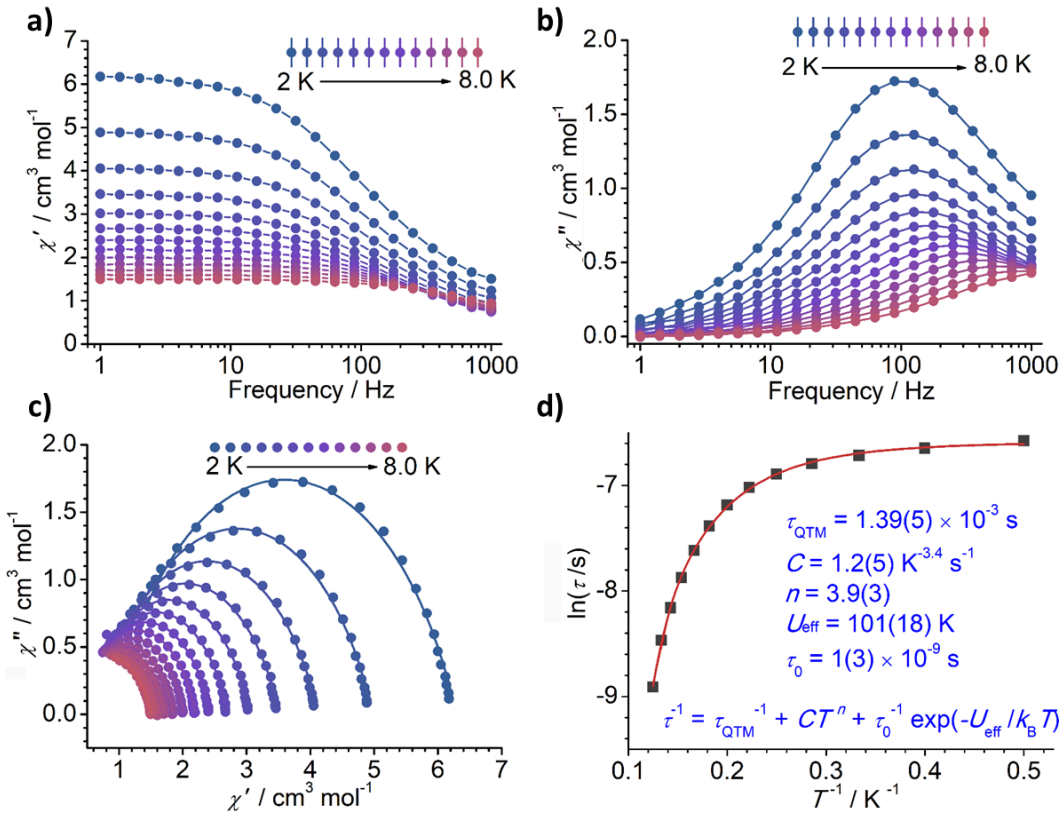

Fig. S18 The in-phase (a) and out-of-phase (b) ac susceptibilities, corresponding Cole-Cole plots (c) and relaxation time (d) of **1UV** under zero field between 2 and 8 K.

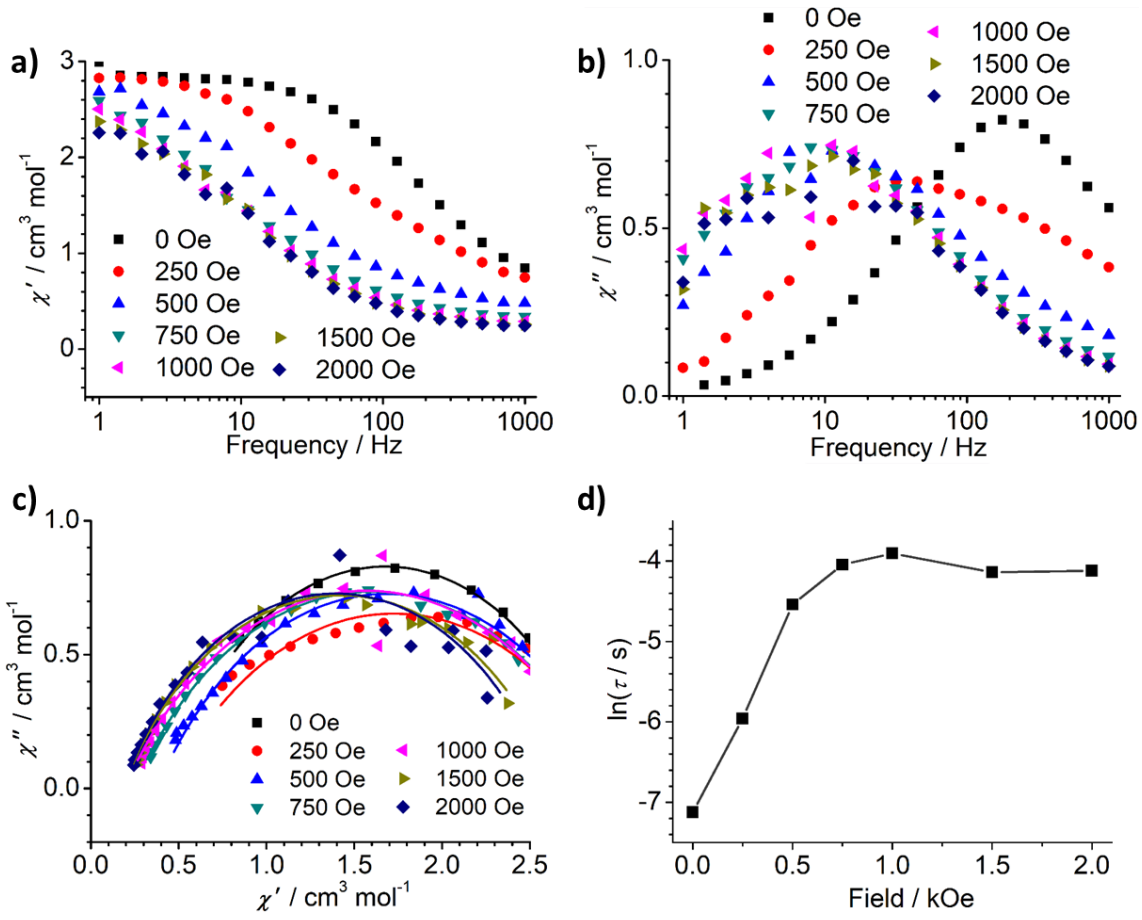

Fig. S19 The in-phase (a) and out-of-phase (b) ac susceptibilities, corresponding Cole-Cole plots (c) and relaxation time (d) of **1UV** at 5 K under different dc field.

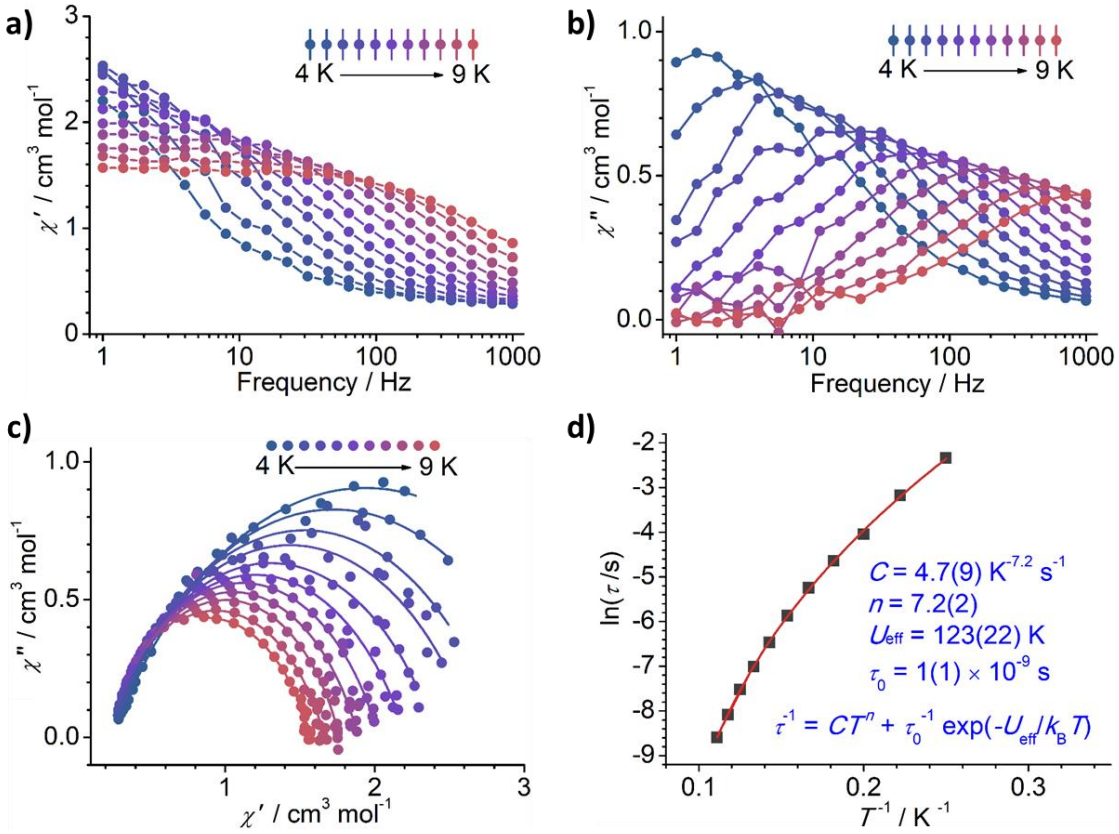

Fig. S20 The in-phase (a) and out-of-phase (b) ac susceptibilities, corresponding Cole-Cole plots (c) and relaxation time (d) of **1UV** under 1 kOe dc field between 4 and 9 K.

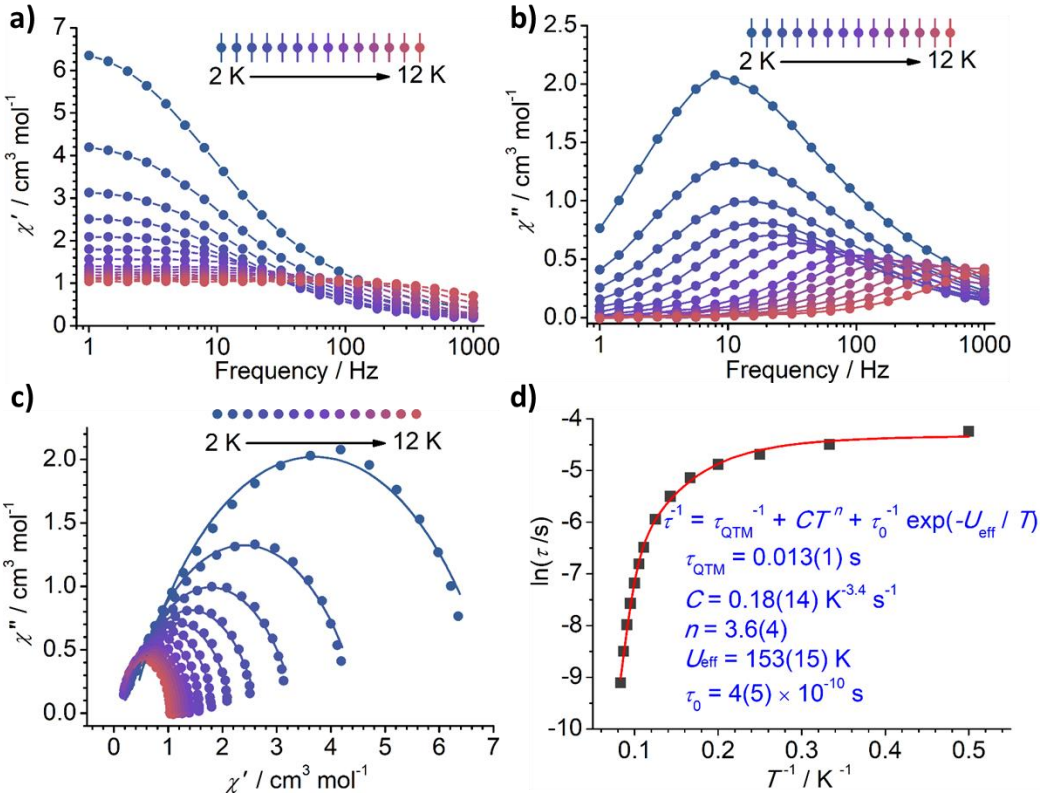

Fig. S21 The in-phase (a) and out-of-phase (b) ac susceptibilities, corresponding Cole-Cole plots (c) and relaxation time (d) of **1R** under zero field between 2 and 12 K.